

Statistical shape analysis of brain arterial networks (BAN)

Xiaoyang Guo*, Aditi Basu Bal*, Tom Needham[†] and Anuj Srivastava *

*Department of Statistics, [†]Department of Mathematics

Florida State University

Abstract

Structures of brain arterial networks (BANs) – that are complex arrangements of individual arteries, their branching patterns, and inter-connectivities – play an important role in characterizing and understanding brain physiology. One would like tools for statistically analyzing the shapes of BANs, i.e. quantify shape differences, compare population of subjects, and study the effects of covariates on these shapes. This paper mathematically represents and statistically analyzes BAN shapes as *elastic shape graphs*. Each elastic shape graph is made up of nodes that are connected by a number of 3D curves, and edges, with arbitrary shapes. We develop a mathematical representation, a Riemannian metric and other geometrical tools, such as computations of geodesics, means and covariances, and PCA for analyzing elastic graphs and BANs. This analysis is applied to BANs after separating them into four components – top, bottom, left, and right. This framework is then used to generate shape summaries of BANs from 92 subjects, and to study the effects of age and gender on shapes of BAN components. We conclude that while gender effects require further investigation, the age has a clear, quantifiable effect on BAN shapes. Specifically, we find an increased variance in BAN shapes as age increases.

1 Introduction

The human brain is one of the most sophisticated organs in human body and serves as the center of the nervous system. It requires significant amount of energy to accomplish its tasks and a complex network of arteries is used to supply the necessary oxygen and energy to brain parts. Thus, this network, called *Brain arterial network* or BAN, is central to maintaining normal anatomical functionality of the brain and its parts. The structure or morphology of BANs determines its effectiveness in providing supply lines, and in characterizing and diagnosing brain health. Consequently, a statistical analysis of shapes of BANs, which constitutes representing and analyzing shape variability within and across human populations, is an important problem area. However, this analysis is difficult because the BANs have complicated structures, with tremendous variability in terms of branching, winding, and merging nature of arteries on one hand, and the shapes and sizes of arteries on the other.

Some examples of BANs for different human subjects are shown in Fig. 1 and later in Fig 2. Each BAN is reconstructed from a 3D Magnetic Resonance Angiography (MRA) image using a tube-tracking vessel segmentation algorithm [1, 2]. In view of the complex nature of BANs, previous analyses have primarily focused on first extracting some low-dimensional features from the original data, followed by a statistical analysis of these features. One of the earliest analyses [5] focused on some simple geometrical summaries, such as the numbers and the lengths of the arteries. More recently, the features have become more sophisticated. For instance, [3] uses tools from Topological Data Analysis (TDA), where one extracts certain mathematical features (e.g., *persistent homology*) from the data and compares these features using certain metrics [40]. However, the difficulty in such *feature-based* approaches is that these representations are typically not invertible. Feature extraction usually represents only partial information about the original objects, forming a many-to-one mapping (from the object space to a feature space) and it is not clear as to which set of shapes share the same topological features. Due to this lack of invertibility, it is difficult to map solutions or statistical inferences back to the object space. In this paper we take a more ambitious approach, where

we develop a statistical analysis of BANs in the original space itself, without resorting to extracting any features. In the process we seek solutions – shape summaries, shape PCA, and shape models – that can be studied as BANs themselves.

While BANs are interesting in themselves, there are other biological and anatomical objects with similar shape architectures, displaying complex filamentary shapes. Examples include retinal blood vessels [16], vein structures in fruit fly wings [34] and neurons [25]. A defining characteristic of these objects is that they are composed of a network of 3D curves, each with arbitrary shapes and sizes, that merge and branch at arbitrary junctions and result in intricate patterns of pathways. While we mainly focus on BANs in this paper, the framework presented here is generally applicable to these other application areas also. Statistical shape analysis of such objects is difficult because in order to quantify shape differences one needs to take into account the numbers, locations, branchings, and shapes of individual curves. In particular, one has to solve a difficult problem of *registration of points and parts* across objects, *i.e.* which points on a branch on one object matches with which points or parts on the other.

The field of shape analysis has steadily gained in relevance and activity over the last two decades. This rise is fueled by the availability of multimodal, high-dimensional data that records objects of interest in a variety of contexts and applications. Shapes of objects help characterize their identity, classes, movements, and roles in larger scenes. Consequently, many approaches have been developed for comparing, summarizing, modeling, testing, and tracking shapes in static image or video data. Statistical shape analysis requires mathematical representations and proper metrics. While early methods generally relied on discrete representations of shapes [23, 22, 33, 10], more recent methods have focused on continuous objects such as scalar functions [36], Euclidean curves [42, 24, 43, 36], and 3D surfaces [21]. The main motivation for this paradigm shift comes from the need to address *registration*, considered the most challenging issue in shape analysis. Registration refers to establishing a correspondence between points or features across objects and is an important ingredient in comparing shapes. Continuous representations of objects use convenient actions of the parameterization groups to help solve dense registration problems. Furthermore, they use elastic Riemannian metrics – which are invariant to the actions of re-parameterization groups – and some simplifying square-root representations, to develop very efficient techniques for comparing and analyzing shapes.

While elastic Riemannian shape analysis is considered well developed for elementary objects – Euclidean curves [43, 35], manifold-valued curves [45, 28], 3D surfaces [20], trees [11, 39] – the problem of analyzing more complex objects remains less explored. Stated differently, the past work has mainly focused on objects that exhibit only the geometrical variabilities, while being of same or similar topologies. Similar topologies help pose the registration problem as that of optimal (diffeomorphic) re-parameterization of the common domain. In this paper we are concerned with comparing BANs that can potentially differ in both topologies and geometries.

Specific Goals: Our goal here is to develop a suite of techniques for statistical analysis of BAN shapes. Specifically, we seek: (1) a **shape metric** that is invariant to the usual shape-preserving transformations, (2) elastic **registration** of parts across BANs, (3) computation of **geodesic** paths between any two BANs and (4) computation of **statistical summaries** – mean, covariance, PCA, etc – in the shape space of BANs. These tools, in turn, can be used for analysis, clustering, classification, and modeling of shapes in conjunction with other machine learning methods. We reiterate that existing techniques may provide some but not all of these solutions.

Our approach is to view BANs as extensions of traditional graphs with the usual node-edge representations. The difference lies in that edge characterization is now more sophisticated – each edge is a full shape of a curve connecting the corresponding nodes, as shown in the right panel of Fig. 1. These graphs, called *elastic graphs*, are represented by their adjacency matrices, with matrix elements given by the shapes of the corresponding edges. Since the ordering of nodes in these graphs, and subsequent indexing of adjacency matrices, is arbitrary we model this variability using an action of the permutation group, and represent each shape as an orbit under this group. Then, we develop techniques for optimization under this permutation group (also known as *graph matching*), leading to computations of geodesics and summaries under the induced metric on the Riemannian quotient space, termed the *graph shape space*. There is no currently existing geometrical framework for shape analysis of such graphical objects. While TDA and other such methods can provide a measure of dissimilarity in shapes, this paper provides more comprehensive statistical quantities such as mean, covariance, principal modes, etc, for a more faithful shape summarization and modeling.

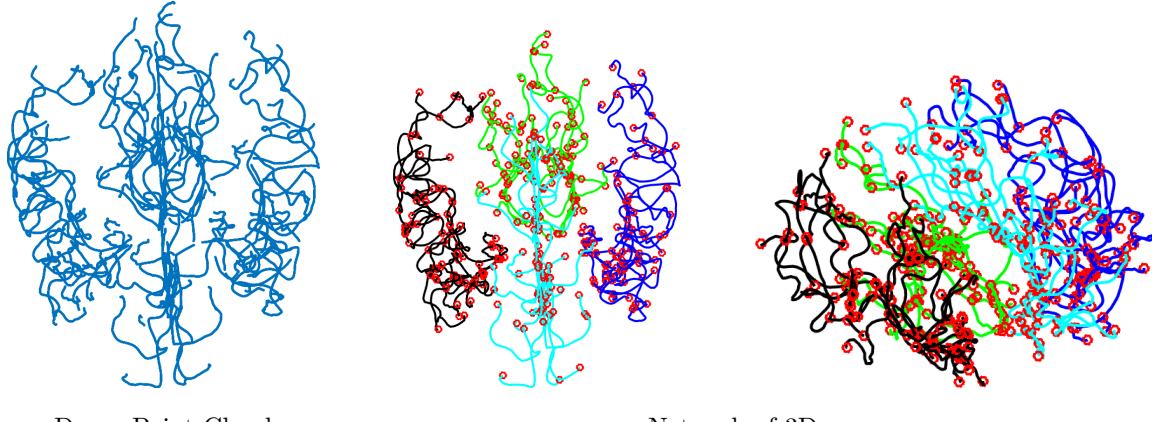


Figure 1: Different representations of BAN data. The four components: top, left, bottom, and right are shown in cyan, black, green, and blue, respectively. Nodes are denoted by red circles.

In order to further tame the complexity and to improve registration results, we break a BAN into four components – top, bottom, left, and right – as shown in different colors on the right side of Fig. 1. Then, we study each of these components individually. Figure 2 shows some examples of these four components from different subjects.

2 Proposed Mathematical Framework

We now present a mathematical framework for representing elastic graphs, keeping in mind that BAN components are the motivating data. The proposed framework can be viewed as an extension of some previous works on graphs [7, 8, 14, 17, 18, 19]. However, those past works are restricted to only scalar-weighted graphs and do not consider more sophisticated features such as shapes.

2.1 Elastic Graph Representation

We are interested in objects that are made of a number of 3D curves, with arbitrary shapes and placements, that merge and branch at arbitrary junctions, and result in a complex network of pathways. We will represent them as graphs with nodes corresponding to junctions and edges corresponding to the shapes of 3D curves connecting the nodes. Here we assume that any two nodes are connected by at most one curve. An edge attributed graph G is an ordered pair (V, a) , where V is a set of nodes and a is an edge attribute function: $a : V \times V \rightarrow \mathcal{S}$. \mathcal{S} is the shape space of elastic 3D curves that is briefly discussed next.

The edges in elastic graphs are Euclidean curves and to analyze their shapes we use elastic shape analysis framework described in [36]. Let $\beta(t) : [0, 1] \rightarrow \mathbb{R}^n, n = 2, 3$, represent a parametrized curve. Define the square root velocity function (SRVF) of β as: $q(t) = \frac{\dot{\beta}(t)}{\sqrt{|\dot{\beta}(t)|}}$, if $|\dot{\beta}(t)| \neq 0$ and zero otherwise. One can recover β from its SRVF using $\beta(t) = \beta(0) + \int_0^t q(s)|q(s)|ds$. If β is absolutely continuous, the SRVF is square-integrable, *i.e.*, $q \in \mathbb{L}^2$. It can be shown that the \mathbb{L}^2 norm on SRVF space is an elastic Riemannian metric on the original curve space. Therefore, one can compute the elastic distance between two curves β_1, β_2 using $d(\beta_1, \beta_2) = \|q_1 - q_2\|_{\mathbb{L}^2}$. One of the most import challenges in shape analysis is registration issue, *i.e.*, finding the point correspondence between curves. Let $\gamma : [0, 1] \rightarrow [0, 1]$ represent a boundary-preserving diffeomorphism. The action of diffeomorphism group on an SRVF q is $q * \gamma = (q \circ \gamma)\sqrt{\dot{\gamma}}$. It is the same as the SRVF of the re-parameterized curve: $\beta \circ \gamma$. To register points across curves, one mods out this re-parametrization group as follows. Each shape can be represented by orbits under the re-parametrization group: $[q] = \{q * \gamma | \gamma \in \Gamma\}$. The set of all orbits is the shape space of curves in \mathbb{R}^n is denoted $\mathcal{S} = \{[q] | q \in \mathbb{L}^2\}$. The metric for shape space is: $d_s([q_1], [q_2]) = \inf_{\gamma} \|q_1 - (q_2 * \gamma)\|$. One can use this metric to define and

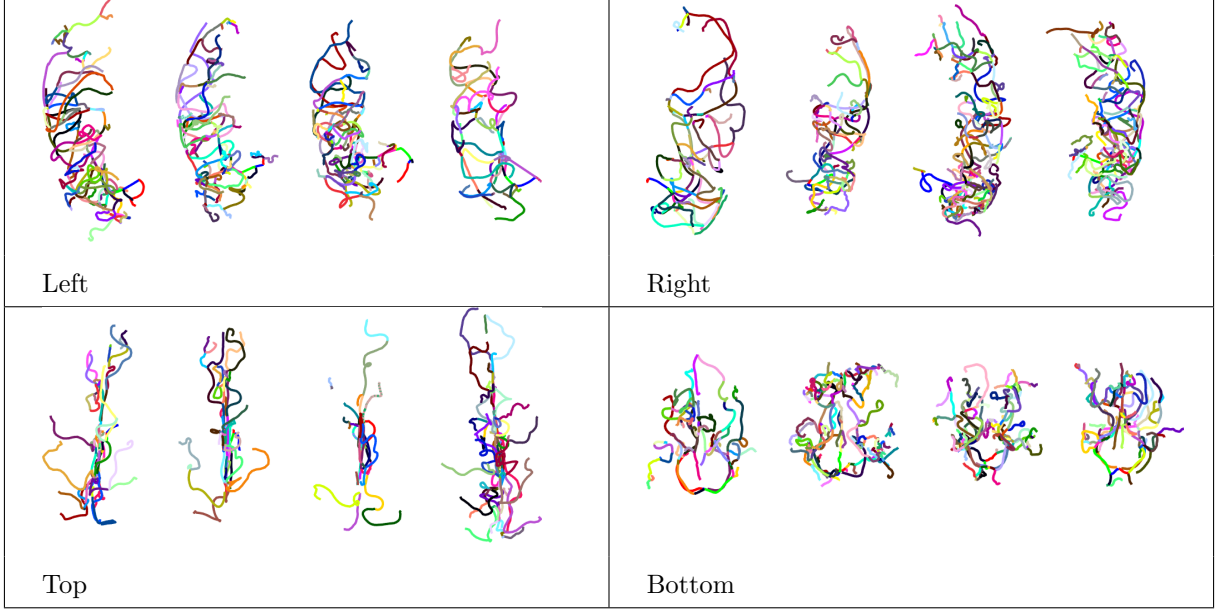


Figure 2: Examples of different four components in BANs.

compute averages of shapes of curves and their PCA analysis. For further details, we refer the reader to the textbook [36].

Remark 1. Note that traditionally one further removes the rotation and scale of curves from considerations in shape analysis, but here these two variables are integral to the shapes of arteries and the network as a whole. So, we do not remove them. We do perform a global rotational alignment of the whole BAN when comparing it with another BAN.

Returning to the elastic graph, the shape $a(v_i, v_j) = [q_{ij}]$ characterizes the shape of curve connecting the nodes $v_i, v_j \in V, i \neq j$. Assuming that the number of nodes is n , G can be represented by its adjacency matrix $A = \{a_{ij}\} \in \mathcal{S}^{n \times n}$, where the element $a_{ij} = a(v_i, v_j)$. For an undirected graph G , we have $a(v_i, v_j) = a(v_j, v_i)$ and therefore A is a symmetric matrix. As an example, the adjacency matrix of the first graph shown in

Fig. 3 is given by:
$$\begin{pmatrix} 0 & 0 & 0 & \cdots & 0 \\ 0 & 0 & [q_{23}] & \cdots & [q_{28}] \\ 0 & [q_{32}] & 0 & \cdots & 0 \\ \vdots & \vdots & \vdots & \ddots & \vdots \\ 0 & [q_{82}] & 0 & \cdots & 0 \end{pmatrix}$$
, where $\mathbf{0}$ denotes a null edge. It implies that the corresponding

nodes are not connected and we substitute the constant zero function $\mathbf{0}$ as its shape. We will assume that there are no self loops in BANs and therefore the diagonal entries in A will also be null.

The set of all such adjacency matrices is given by $\mathcal{A} = \{A \in \mathcal{S}^{n \times n} | A = A^T, \text{diag}(A) = \mathbf{0}\}$. We will use this to impose a metric on the representation space \mathcal{A} . That is, for any two $A_1, A_2 \in \mathcal{A}$, with the corresponding entries a_{ij}^1 and a_{ij}^2 , respectively, the metric: $d_a(A_1, A_2) \equiv \sqrt{\sum_{i,j} d_s(a_{ij}^1, a_{ij}^2)^2}$, quantifies the differences between graphs A_1 and A_2 , where d_s the shape metric for curves as defined above. Under the chosen metric, the geodesic or the shortest path between t-eps-converted-to.pdfwo points in \mathcal{A} can be written as a set of geodesics in \mathcal{S} between the corresponding components. That is, for any $A_1, A_2 \in \mathcal{A}$, the geodesic $\alpha : [0, 1] \rightarrow \mathcal{A}$ consists of components $\alpha = \{\alpha_{ij}\}$ given by $\alpha_{ij} : [0, 1] \rightarrow \mathcal{S}$, a uniform-speed geodesic path in \mathcal{S} between a_{ij}^1 and a_{ij}^2 . Note that this solution also provides an optimal registration of points across edges a_{ij}^1 and a_{ij}^2 .

The main issue in this comparison is that the indexing of nodes in a graph is arbitrary and, thus, the previous matching of edges a_{ij}^1 with a_{ij}^2 is also arbitrary. To illustrate this point, Fig. 3 shows the same graphical object several times and imposes a different node indexing every time. As the result, we need to optimally reorder the nodes every time we are comparing two graphs and we use the permutation group for

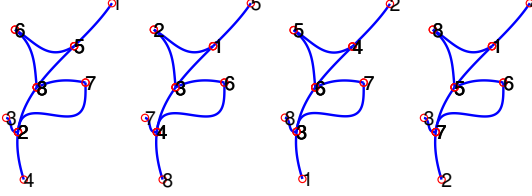


Figure 3: Four graphs with the same shape but with different node labels.

this reordering. A permutation matrix is a matrix that has exactly one 1 in each row and column, with all the other entries being zero. Let \mathcal{P} be the group of all $n \times n$ permutation matrices with group operation being matrix multiplication and identity element being the $n \times n$ identity matrix. We define the action of \mathcal{P} on \mathcal{A} as:

$$\mathcal{P} \times \mathcal{A} \rightarrow \mathcal{A}, P \star A = P \cdot A \cdot P^T. \quad (2.1)$$

Here \cdot implies a permutation of entries of A according to the nonzero elements of P . The action $P \star A$ results in the swapping of rows and columns of A . Under the chosen metric d_a , this mapping is isometric, see Lemma 1.

Lemma 1. *1. Permutation Group: The action of \mathcal{P} on the set \mathcal{A} given in Eqn. 2.1 is by isometries. That is, for any $P \in \mathcal{P}$ and $A_1, A_2 \in \mathcal{A}$, we have $d_a(A_1, A_2) = d_a(P \star A_1, P \star A_2)$.*

2. Global Rotation Group: The action of the rotation group $SO(d), d = 2, 3$ on \mathcal{A} , given by $A \mapsto OA$, or $a_{ij}^1 \mapsto Oa_{ij}^1$, is also be isometries. That is, for any $O \in SO(d)$ and $A_1, A_2 \in \mathcal{A}$, we have $d_a(A_1, A_2) = d_a(OA_1, OA_2)$.

The orbit of an $A \in \mathcal{A}$, under the joint action of \mathcal{P} and $SO(d)$, is given by: $[A] = \{O(P \star A) | P \in \mathcal{P}, O \in SO(d)\}$. Any two elements of an orbit denote exactly the same graph shape, except that the ordering of the nodes has been changed and the graph has been rotated.. The membership of an orbit defines an equivalent relationship \sim on \mathcal{A} :

$$A_1 \sim A_2 \Leftrightarrow \exists P \in \mathcal{P}, O \in SO(d) : O(P \star A_1) = A_2.$$

The set of all equivalence classes forms the quotient space: $\mathcal{G} \equiv \mathcal{A}/(\mathcal{P} \times SO(d)) = \{[A] | A \in \mathcal{A}\}$. Henceforth, we will call \mathcal{G} the *elastic graph shape space*.

Lemma 2. *Since the action of \mathcal{P} on \mathcal{A} is by isometries under d_a , and the joint group $(\mathcal{P} \times SO(d))$ is finite dimensional, the metric d_a descends to the quotient space \mathcal{G} according to:*

$$\begin{aligned} d_g([A_1], [A_2]) &= \min_{P \in \mathcal{P}, O \in SO(d)} d_a(A_1, O(P \star A_2)) \\ &= \min_{P \in \mathcal{P}, O \in SO(d)} d_a(A_2, O(P \star A_1)). \end{aligned} \quad (2.2)$$

Let $(\hat{P}, \hat{O}) = \operatorname{argmin}_{P \in \mathcal{P}, O \in SO(d)} d_a(A_1, O(P \star A_2))$, then A_1 and $\hat{O}(\hat{P} \star A_2)$ are considered to be *aligned and registered*. The shortest path between $[A_1]$ and $[A_2]$ under the metric d_g is given by $[\alpha(t)]$ where $\alpha : [0, 1] \rightarrow \mathcal{A}$ is a geodesic between A_1 and $\hat{O}(\hat{P} \star A_2)$. This shortest path is a geodesic in the sense that each of its component is a geodesic in \mathcal{S} between the registered edges.

2.2 Graph Matching

The problem of optimization over \mathcal{P} , stated in Eqn. 2.2, is known as the *graph matching problem* in the literature and is the most important challenge in the proposed framework. The optimization over $SO(d)$ is straightforward and the result can be obtained using Procrustes method. We will not discuss it further, and will focus only on the graph matching. This matching is in fact an NP complete [41] problem and its global solution cannot be found in a reasonable time as the graph size increases. Instead, one uses relaxation techniques to find an approximate solution, in one of several ways.

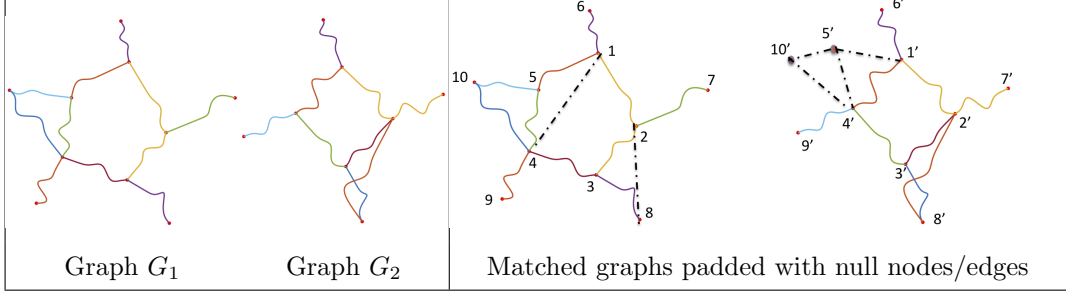


Figure 4: Labeling and addition of null nodes in order to facilitate registration between two graphs.

If the adjacency matrix A were real-valued and edge similarities are measured by the Euclidean norm, then the matching problem can be written as $\hat{P} = \arg \min_{P \in \mathcal{P}} \|A_1 - PA_2P^T\| = \arg \max_{P \in \mathcal{P}} \text{Tr}(A_1PA_2P^T)$. This particular formulation is known as Koopmans-Beckmann's quadratic assignment programming (QAP) problem [26]. One can use an existing relaxation solution for approximating the optimal registration [6, 31, 37, 38].

However, when elements of \mathcal{A} belong to a more general metric space, *e.g.*, shape space \mathcal{S} in this paper, some of the previous solutions are not applicable. Instead, the problem can be rephrased as $\hat{P} = \arg \max_{P \in \mathcal{P}} \text{vec}(P)^T K \text{vec}(P)$. Here $K \in \mathbb{R}^{n^2 \times n^2}$, called an *affinity matrix*, has the following structure. Suppose A_1 has node index a, b, c , etc. and A_2 has node index i, j, k , etc. Then,

- the diagonal entries k_{aiai} measure the affinity between node a of A_1 and node i of A_2 , and
- the off-diagonal entries k_{aibj} measures the affinity between edge ab of A_1 and edge ij of A_2 .

In this paper we use the shape similarity between two edges, obtained using the square-root velocity function (SRVF) representations [35] while modding out the re-parametrization group, as affinity:

$$k_{aibj} = \begin{cases} 0, & \text{if } a_{ab}^1 \text{ or } a_{ij}^2 \text{ is null} \\ \sup_{\gamma} \langle q_1, O(q_2 \circ \gamma) \sqrt{\gamma} \rangle, & \text{otherwise} \end{cases}.$$

Here q_1, q_2 denote the SRVFs of the edges ab of A_1 and ij of A_2 and γ is a diffeomorphic reparameterization. The matrix $O \in SO(d)$ is the global rotation matrix that is used to rotationally align two elastic graphs. (The same O matrix is applied to all the edges of the second graph and minimized using Procrustes rotation.) The resulting formulation is called the *Lawler's QAP probelm* [27]. It can be seen that Koopmans-Beckmann's QAP is a special case of Lawler's QAP. To solve for Lawler's QAP, at least approximately, there are several algorithms available [9, 13, 29, 30, 44, 46, 47]. In this paper, we use the well-known *factorized graph matching* (FGM) algorithm [47] to match elastic graphs.

So far we have assumed that the graphs being matched are of the same size (in terms of the number of nodes). For graphs G_1 and G_2 , with different number of nodes n_1 and n_2 , we can pad them using n_2 and n_1 null nodes, respectively, to bring them to the same size $n_1 + n_2$. As mentioned earlier, null nodes are zero elements in V and any edges attached to the null nodes have zero-valued shapes: $\mathbf{0} \in \mathbb{L}^2$. This way the original (real) nodes of both G_1 and G_2 can potentially be registered to null nodes in the other graph. Figure 4 shows an example of this approach. The left side shows two graphs that have different number of nodes and edges, but still have common structure. On the right side we label the nodes to show a particular matching of these graphs. We obtain this matching by adding two null nodes: $5'$ and $10'$, and corresponding null edges $1' \leftrightarrow 5'$, $10' \leftrightarrow 5'$, $10' \leftrightarrow 4'$, $5' \leftrightarrow 4'$ in G_2 , and the null edges $1 \leftrightarrow 4$, $2 \leftrightarrow 8$ in G_1 .

For the matched graphs, we can compute geodesics by interpolating between the corresponding nodes and edges (according to their respective metrics). We present four illustrative examples in Fig. 5. In each row, we show two graphs G_1 and G_2 drawn as the first and the last graphs in each picture. Additionally, we show a sequence of shapes along the geodesic path between them in two different spaces – \mathcal{A} and \mathcal{G} , i.e., with arbitrary registration and with optimal registration. The deformations between registered graphs, associated with geodesics in \mathcal{G} , look much more natural than those in \mathcal{A} . The edge features are preserved

better in the intermediate graphs along the geodesics in \mathcal{G} . The edges that are unmatched between the two graphs disappear or appear along the geodesic. The top two rows are for a 2D graph while the remaining are 3D graphs. As mentioned earlier, the points along registered edges of graphs are also registered while computing d_s . Thus, we have a dense (complete) registration of parts across the two graphs and it makes the deformation appear more natural.

3 Shape Summaries of Elastic Graphs

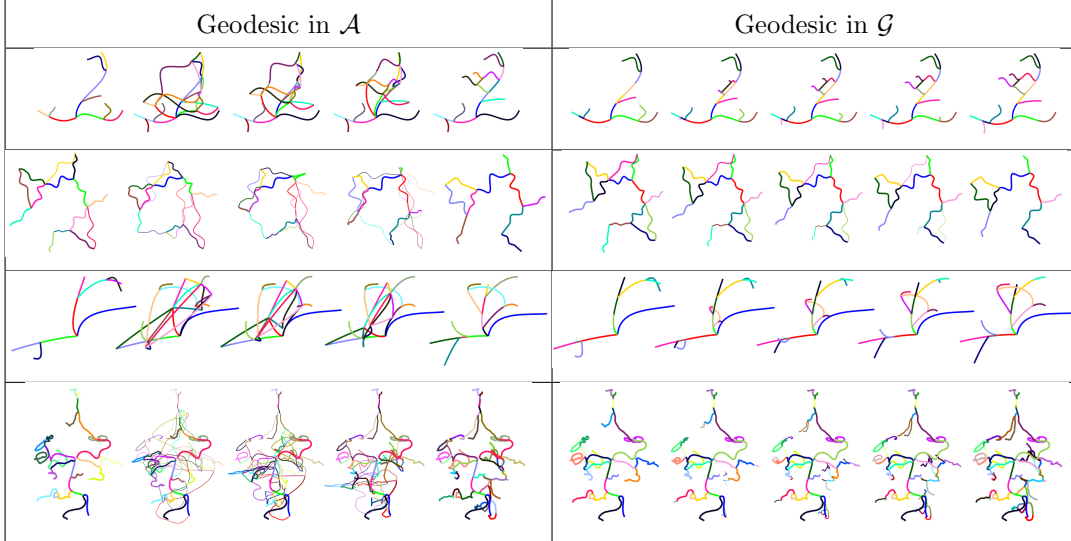


Figure 5: Geodesic between graphs in space \mathcal{A} (left) and the \mathcal{G} (right). Coloring is used to depict registration of edges across graphs. The top two rows show 2D graphs while bottom two use 3D graphs. (Gif animations of these geodesics are provided with the supplementary material.)

Given BAN datasets, we are interested in tools that facilitate statistical inferences, such as classification, clustering, hypothesis testing, and modeling. The use of a metric structure to compute summaries of shapes of graphs is of great importance in these analyses. We will use the metric structure introduced earlier to define and compute shape statistics – such as mean, covariance, and PCA – of given graph data. Further, we will use these representations to perform dimension reduction and hypothesis testing.

3.1 Mean Graph Shapes

Given a set of graph shapes $\{[A_i] \in \mathcal{G}, i = 1, 2, \dots, m\}$, we define their mean graph shape to be:

$$[A_\mu = \arg \min_{[A] \in \mathcal{G}} \left(\sum_{i=1}^m d_g([A], [A_i])^2 \right),$$

where d_g is as defined in Eqn. 2.2. There are at least two different ways for finding this mean. One relies on the gradient of the cost function in this optimization, and the other relies on finding a sequence of geodesic paths.

Method 1 – Gradient Approach: The gradient-based algorithm for computing the mean shape is given in Algorithm 1. Note that this gradient solution is a local minimum of the functional and does not guarantee a global minimizer.

We present an example of computing mean graphs in Fig. 6. The left side shows a set of 12 graphs whose mean is being computed. While these graphs have a common skeletal structure – a ringlike interior with radial offshoots – they also differ significantly in terms of the number of nodes/edges and shapes of

Algorithm 1 Graph Mean in \mathcal{G}

Given adjacency matrices A_i , $i = 1, \dots, m$:

- 1: Initialize a mean template A_μ (e.g., the largest one).
- 2: Match A_i to A_μ using FGM [[47] and SRVF [36], store the matched graph shape as A_i^* , for $i = 1, \dots, m$.
- 3: Update $A_\mu = \frac{1}{m} \sum_{i=1}^m A_i^*$.
- 4: Repeat 2 and 3 until $\sum_{i=1}^m d_a(A_i^*, A_\mu)^2$ convergence.

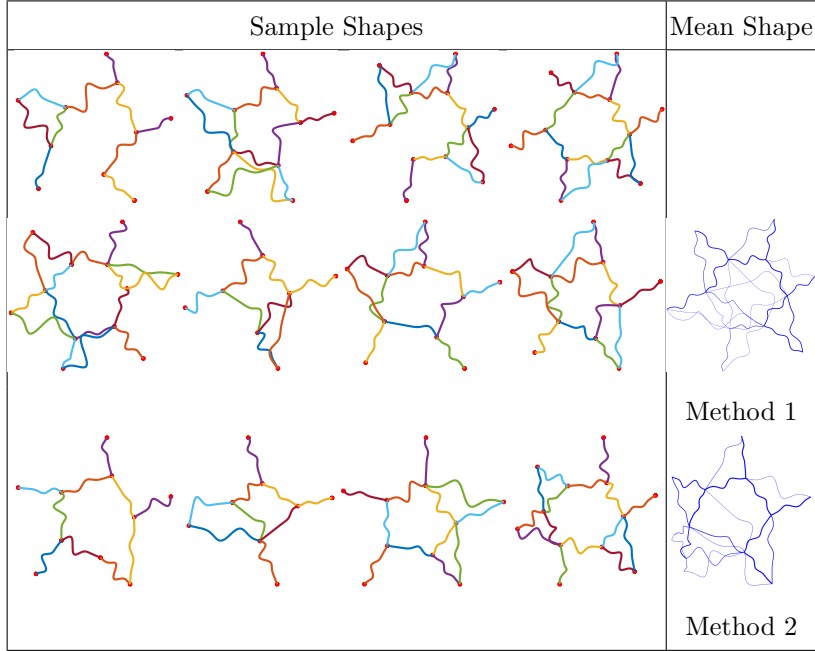


Figure 6: Left side shows 12 sample graphs and the right column shows their sample means computed using two different methods. The thickness of edges in the mean shape represents how often an edge is present in sample shapes.

edges. The mean of these graphs, computed using this method, is shown in top right of the figure. It is a good representative of the samples graphs, capturing the overall ringlike skeleton. The thickness of edges in the mean graph represent the frequency with which they appear in the given samples. Once can prune thin edges to focus on the overall common structures.

Method 2 – Sequential Approach: In this approach, one starts with two graphs at a time computes their mean and updates it using one additional individual graph at a time. The full algorithm is given below.

The bottom right panel of Fig. 6 shows the result of computing mean shape using Algorithm 2. This is the mean of 12 shapes shown on the left side of this figure. Comparing this mean shape with the mean compute using Algorithm 1, shown in the top right of this figure, we see a lot of structural similarities. Also, we see some visible differences in the shapes of individual edges across the two means. Ideally, these two results should be identical but numerical optimizations involved in different steps of these procedures, especially Algorithm 1, leads to these smaller differences.

3.2 Tangent PCA in Graph Shape Space

Graphical shape data is often high dimensional and complex, requiring tools for dimension reduction for analysis and modeling. In past shape analysis, the tangent PCA has been used for performing dimension

Algorithm 2 Graph Mean in \mathcal{G}

Given adjacency matrices $A_i, i = 1, \dots, m$:

- 1: Find the constant speed geodesic between A_1 and A_2 and set μ to be the halfway point.
- 2: For each $i = 3, 4, \dots, m$, find the constant speed geodesic between μ and A_i . Set μ to the point at $\frac{1}{i}$ th distance from the previous μ along that new geodesic.

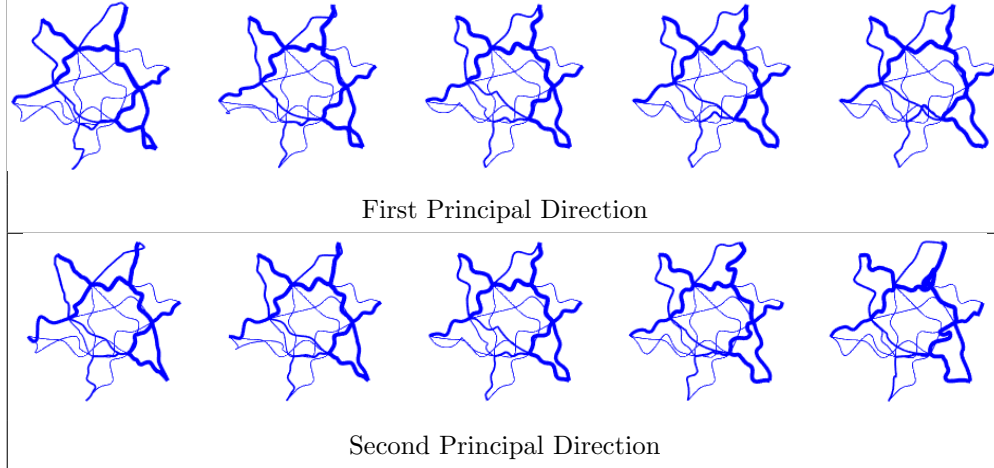


Figure 7: Variation of simulated elastic graphs along the two principal directions. In each row, the middle shape is the mean while the right sides and left sides are perturbation from mean by $\pm 1, \pm 2$ square-root of the singular values.

reduction and for discovering dominant modes of variability in the shape data. Given the graph shape metric d_g and the definition of shape mean A_μ , we can extend TPCA to graphical shapes in a straightforward manner. As mentioned earlier, due to the non-registration of nodes in the raw data the application of TPCA directly in \mathcal{A} will not be appropriate. Instead, one can apply TPCA in the quotient space \mathcal{G} , as described in Algorithm 3. After TPCA, graphs can be represented using low-dimensional Euclidean coefficients, which facilitates further statistical analysis.

Algorithm 3 Graph TPCA in \mathcal{G}

Given adjacency matrices $A_i, i = 1, \dots, m$:

- 1: Find the mean A_μ using Algorithm 1 or 2. They results in the mean and the registered graphs $A_i^*, i = 1, 2, \dots, m$.
- 2: For each i , evaluate the shooting vectors $v_i = (A_i^* - A_\mu)$ as elements of $T_{A_\mu}(\mathcal{G})$ (the tangent space at A_μ).
- 3: Perform PCA using the shooting vectors $\{v_i, i = 1, 2, \dots, m\}$ in $T_{A_\mu}(\mathcal{G})$. Obtain principal directions and singular values for the principal components.

An example of this TPCA procedure for graphical shapes is shown in Fig. 7. The data used here is the same as that in Fig. 6 and the figure shows shape variability along the first principal direction. As we can see, the first principal direction mainly changes of shapes of the smaller edges, since the largest path is essentially the same across all the graphs.

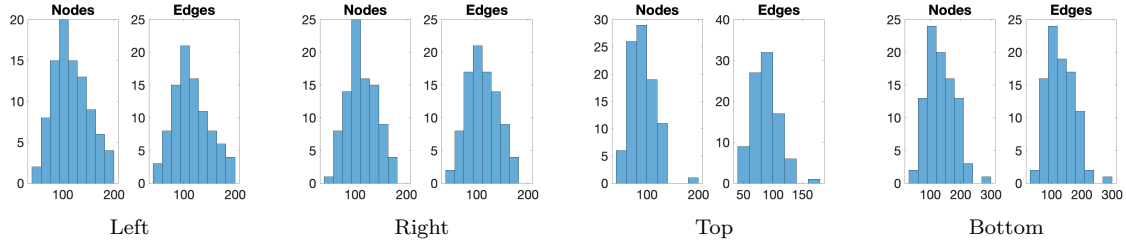


Figure 8: Histogram of number of nodes and edges in four components. $N = 92$.

4 Brain Artery Trees

Having developed tools for registering, comparing, and summarizing graphs using means and covariance, we now turn our attention to analysis of BAN data [4].

We study the data from a geometric point of view and analyze full shapes of these brain networks. From an anatomical perspective, it seems natural to divide the full network into four components, as shown in Fig. 1. This division helps us focus on comparisons of individual components across subjects and also makes the computational tasks more efficient. The original data has 98 subjects but we remove six subjects that are difficult to separate into components, resulting in a sample size of $N = 92$. In Fig. 8, we provide some relevant statistics on the numbers of nodes and edges in the four components over the selected sample. As these histograms show, these graphs differ drastically in terms of the numbers of nodes and edges across subjects. Additionally, there are large differences in both the shapes and the patterns of arteries forming these networks. Consequently, the problem of analyzing shapes of these BANs is quite challenging, and remains relatively unexplored in the past.

4.1 Node Matching Accuracy in BANs

As emphasized several times earlier, matching of nodes (and edges) across graphs is the most important bottleneck in shape analysis of elastic graphs. Since the state-of-art solutions are approximate at best, one needs to investigate the quality of these results in our contests. Here we present some experimental results on node matching in BANs using simulated data. We randomly select a BAN from the database and apply a random permutation to the ordering of its nodes. To further complicate this task we remove edges in the permuted graph (independently) with probability p . Then, we use the FGM algorithm to match the nodes of the new graph with those of the original graph. To evaluate the result, we compute the proportion of estimated matches that match with the original order. We repeat this process 20 times for all the four components and compute a summary of the results presented in Fig. 9. Each plot shows the correction matching proportion, as a function of p , for the four BAN components. Notably, for $p = 0$, *i.e.* when the two graphs are identical, the algorithm fully recovers the original ordering. Even when the 10% of shapes are removed, the algorithm finds correct ordering of the original nodes at 90% proportion. While the real application is more challenging, because one is comparing different BANs at any time, these experiments provide some confidence in the node matching results obtained in our framework.

4.2 Geodesic Deformations

Next, we use the techniques developed in this paper to compute geodesic paths between arbitrary BAN components and present some pictorial examples in Fig. 10. The first column in each row shows a full geodesic for a BAN component of one subject to another, as elements of \mathcal{G} . To improve visual clarity we remove some unmatched edges from the graphs and plot the same geodesic again in the right column. We have used color coding of edges to show registration and to track the deformation of each edge. These geodesics are useful in several ways. They provide registrations of arteries across networks and they help follow deformations of matched arteries from one network to another.

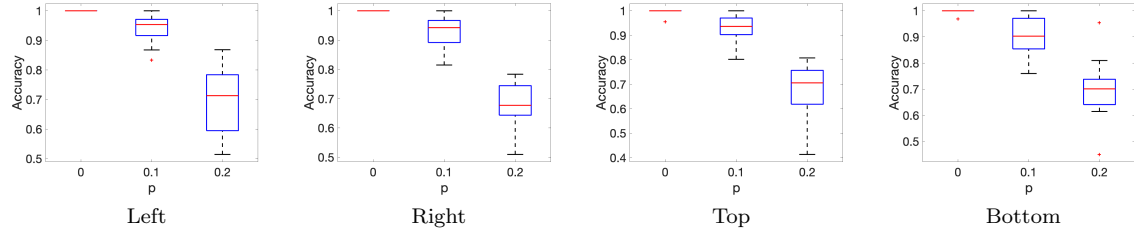


Figure 9: Matching accuracy of brain arteries networks. The horizontal axes are the probability p for deleting edges.

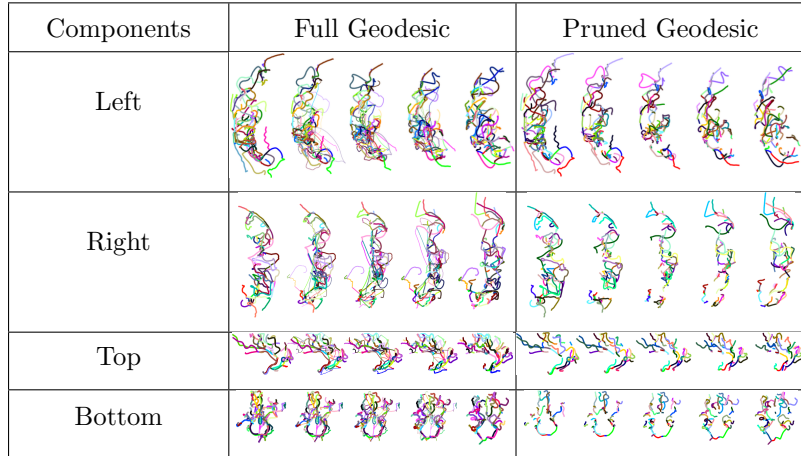


Figure 10: Geodesics between BAN components. In each row we first show the full geodesic and then show a pruned geodesic where the unmatched edges are dropped.

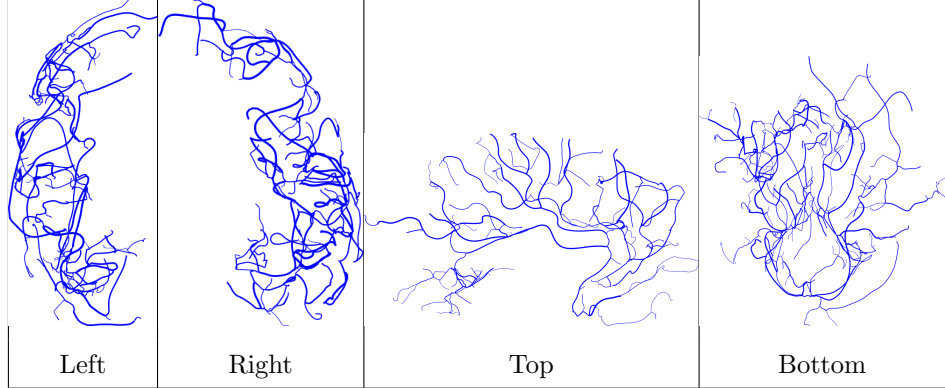


Figure 11: Average shapes of BAN components across 92 subjects. Thickness of edges is represents its proportional presence in individual subjects – a thicker edge indicates it is present in more subjects.

4.3 Average BAN Shapes

Given 92 sample BANs, it is interesting and useful to be able to compute their mean shape. Since the computational cost of pairwise matching of graphs is high, the computation for an average graph, using Algorithm 1 becomes very expensive. To accelerate this process, we use the following approximation. We basically register each graph shape to the largest size graph in the dataset and used that fixed registration to compute the mean. This is not quite the optimal registration prescribed in Algorithm 1 but it provides a decent approximation.

Figure 11 shows the mean shapes for all the four components across 92 subjects. Since these 92 graphs differ in the number, connectivities, and shapes of edges, it is a little difficult to visualize and interpret the mean shapes. One really needs to view 3D displays of these shapes to appreciate how well these means capture the common structures in individual graphs. We use thickness of edges to denote the proportion of individual graphs in which that particular edge is present. As expected, these mean shapes show a smoother, higher-level representation of individual shapes and largely preserve connectivity patterns present in the data.

The computation of an average shape is an important, novel result and has not been achieved for BANs or similar graph data before. Its importance lies in our need to separate between structures that are common across subjects and structures that distinguish subjects from each other. By separating this variability, one can focus on individual differences and try to capture this variability using regression models. Structures that are common to all subjects are removed from the analysis, greatly simplifying the ensuing statistical analysis. We present these studies in the next few sections.

4.4 PCA-Based Analysis of Covariate Effects on Shape

An important use of the proposed framework is in understanding the the effects of covariates, such as gender and age, on shapes of BANs. Due to the high dimensionality and complex nature of BANs, this task is nearly impossible in this original formulation. We use the elastic shape analysis framework to compute average shapes, extract individual variability, and focus on modeling this individual variability against the covariates. As earlier, we do this component wise, *i.e.* a separate analysis of each component of BAN.

We first perform Graph PCA using Algorithm 3 on BAN components and represent each individual subject data into a low-dimensional vector space via projection. A BAN component with 197 nodes and 50 discrete points in each edge has a discrete representation with $3 \times 50 \times 197 \times 197 = 5821350$ elements. However, using Graph PCA, we can retain 80% of the variability in the original data using only 60 principal components. In order to avoid the confounding effect of artery size, we rescale edges by the total artery length. As the result, we can focus on gender and age effects on the shapes of BANs.

Table 1: Testing of gender effect on principal scores of shapes of brain arterial networks.

	t test	Hotelling's T-squared test			
		PC 1-2	PC 1-3	PC 1-4	PC 1-5
Left	0.1354	0.5228	0.4333	0.5074	0.4009
Right	0.8868	0.0785	0.1630	0.0792	0.1210
Top	0.9236	0.6788	0.0676	0.1200	0.1400
Bottom	0.4005	0.0599	0.1256	0.1447	0.2328

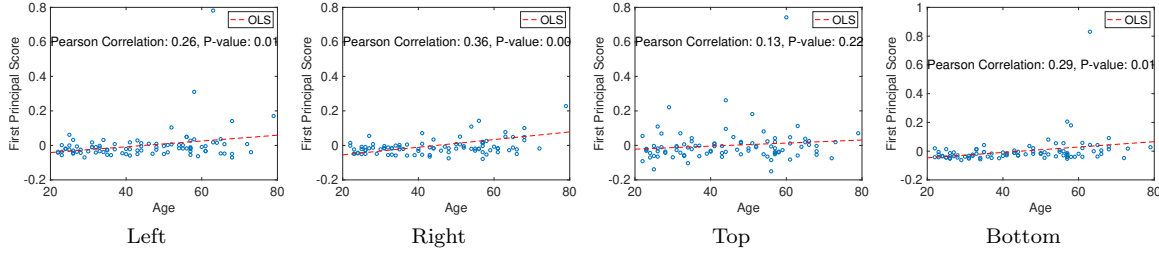


Figure 12: Correlation between ages and first principal scores of shape of arterial networks.

4.4.1 Gender Effect on BAN Shapes

To study the effect of gender on the arterial graph shapes, we implement a two sample t-test on the first principal scores and a Hotelling's T-squared test on the first several principal scores. The resulting p -values can be found in Table 1. Most of the p -values are high, thus we do not find any significant difference between shapes of BANs and the gender. To further investigate this result, we also applied a permutation test (described in the following paragraphs) and obtained similar results; see Table 2. We note that [3] and [32] reported multiple insignificant and significant p -values on the same data using completely different mathematical representations. Whether there is an anatomical shape difference between brain arterial networks of female and male subjects remains an open question and needs further investigation.

4.4.2 Age Effects on BAN Shapes

To study the effect of age of a subject on the shape of his/her BAN, we studied correlations between the age and the PCA scores of arterial shapes. The results are shown in Fig. 12. We found a strong linear correlation between age and first principal scores of brain arteries in most cases (all except the top component). The correlation coefficients between the principal shape score for the left, right, and bottom components and ages are 0.26, 0.36, and 0.29 respectively. All of them are significant with p -values almost zero. This result is similar to some published results in the literature but obtained using different mathematical representations than ours [3, 32]. The difference lies in our ability to visualize the nature of deformations resulting from the age effect. As mentioned before, we also use a permutation test to validate the age effects.

An important question is: How do the BAN shapes change as a subject gets older? The tools developed in this paper can be used to visualize the aging effect on the shape of brain arteries, while feature-based methods proposed in the past cannot address this question. Using Algorithm 3, we compute PCA scores for each BAN shape. Treating these scores as a response and the age as a predictor, we fit a zero-mean model to the data. Note that since principal scores can be used to reconstruct original graphs, we have a way of mapping these representations into graphs for visualizations. Therefore, we can visualize the effects of aging on the shapes of BANs as in Fig 13. Here we fit a linear model using age to predict the first principal scores. To facilitate better visualization of where the changes are occurring, we calculate the edgewise shape differences using the mean shape as baseline and use red color to denotes edges with large deformations, *i.e.*

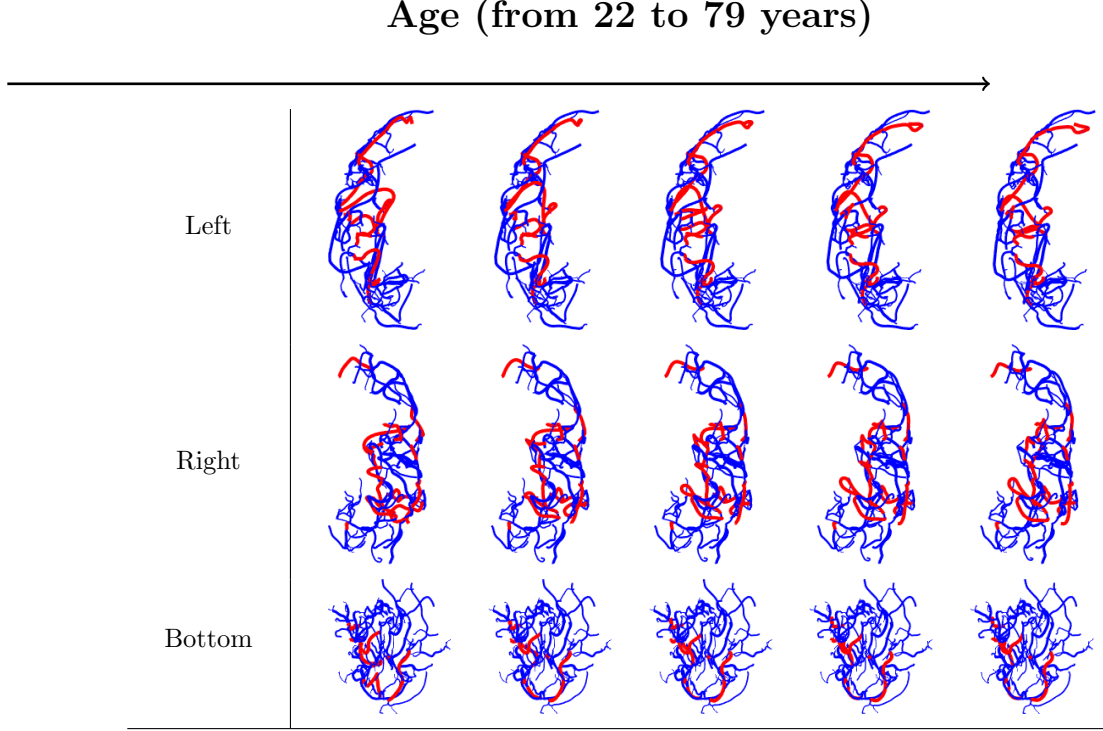


Figure 13: Aging effect on brain arteries. For each component, from left to right is the mean shape deformation when going from age 22 to 79. The red color highlights edges that have large deformations.

deformations that are greater than 50% of the differences.

4.5 Metric-Based Study of Covariates Effects on Shapes

We also investigate the effects of covariates on full BAN shapes using the shape metric d_g (Eqn. 2.2) directly. Fig. 14 shows matrices of pairwise distances between subjects, one matrix for each four components separately. (As mentioned before, we have scaled the edges by the total artery length and thus the distances quantify only shape differences.) We reorder the distance matrices by the ages of subjects, to help elucidate the effect of aging on shape variability. The color pattern of pixels in these matrices show that shape distances increase with the age (darker red colors are towards bottom right). This implies that the shape variability in brain arterial networks grows with the age for three of the four components. This pattern does not hold for the top component.

To further validate the gender and age effects, we implement a permutation test [[15] based on shape

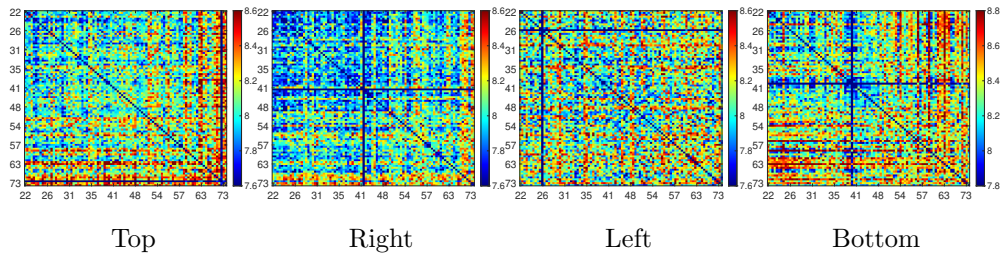


Figure 14: Matrices of shape distances between BAN components of 92 subjects. The axes are labeled by ages.

Table 2: Permutation test of gender and age effect on distances of shapes of brain arterial networks.

	Left	Right	Top	Bottom
Gender	0.0385	0.2128	0.4835	0.0706
Age	0.0006	0	0.4772	0

metric d_g . The basic idea is as follows. We divide the subjects into two groups – older than 50 and younger than 50 – and compute the test statistics specified in [[15]]. Then, we repeat this process $30K$ times, each time randomly assigning subjects into different groups and computing the test statistics. Using a histogram of the $30K$ test statistics, we can compute the p -value of real-data test statistic. The result can be found in Table 2. While the gender effect still remains unclear, one can see a significant age effect on the brain arteries for the left, right, and bottom components. We also see that the top component remains relatively unchanged between young and old people. (We remind the reader that the pairwise distance is compromised because of computational cost. Here we first match each graph to the largest graph in the dataset and compute pairwise shape distances without any further matching.)

5 Improving Registration Using Landmarks

The problem of matching parts of BANs is the most important bottleneck in shape analysis of elastic graphs, as stated earlier. The procedure laid out so far for graph matching is fully automated but in the end does not guarantee a global solution. One can potentially improve this solution in case there is some extra matching information. This knowledge can be in form of some prominent points, called *landmarks*, that have known registrations across graphs. In this context, two issues arise: (1) Where can the landmarks come from?, and (2) How to incorporate this extra information in improving dense registration of graphs?

For the first issue, there are several possibilities. The landmarks may be provided by the domain experts using manual data analysis. Another possibility is to perform a preliminary investigation of the data and extract some landmarks of interest first. Then, use specialized techniques to register only the landmarks first. To facilitate this approach, one can use tools from traditional graph-theoretic analysis to automatically discover and extract some prominent landmarks. Examples of relevant tools include multi-resolution representations of graphs, clustering of nodes using graph spectra, and Dijkstra’s method for finding the longest paths in a graph. For instance, one can use the longest arteries in BANs, and some prominent nodes along with them, as landmarks for matching across BANs.

The second issue – how to incorporate given landmarks registration in solving Eqn. 2.2 – is more methodological. We will assume that all landmarks are *nodes* in the original graphs, although one can relax this assumption at the cost of some increased computational complexity. For these *registered nodes*, the corresponding entries of $P \in \mathcal{P}$ are fixed and no longer part of the search. Assuming $n_0 \leq n$ to be the number of landmarks, the search space is now reduced to $(n - n_0) \times (n - n_0)$ permutation matrices. This constrained search has also been called *seeded graph matching* in the literature [12].

We present an example of landmark driven matching in Fig. 15. In this example, we study two BAN component (bottom) shown in the figure. We use five landmarks – one at a central node and two each placed automatically along the two longest paths in the graph starting from the central node – to perform improved registration of the graphs. The resulting geodesic is presented in the top row. We prune this display by removing the unmatched edges and show the pruned geodesic in the bottom row. In this example, the geodesic distance before using landmarks is 244.1698 but comes down to 237.3467 after using landmarks-based matching, signifying an improvement in registration of nodes. We demonstrate an example of landmark-based matching and mean computation in Fig. 16. The use of landmarks improves the registration and thus keeps the major patterns (two longest paths) for the mean.

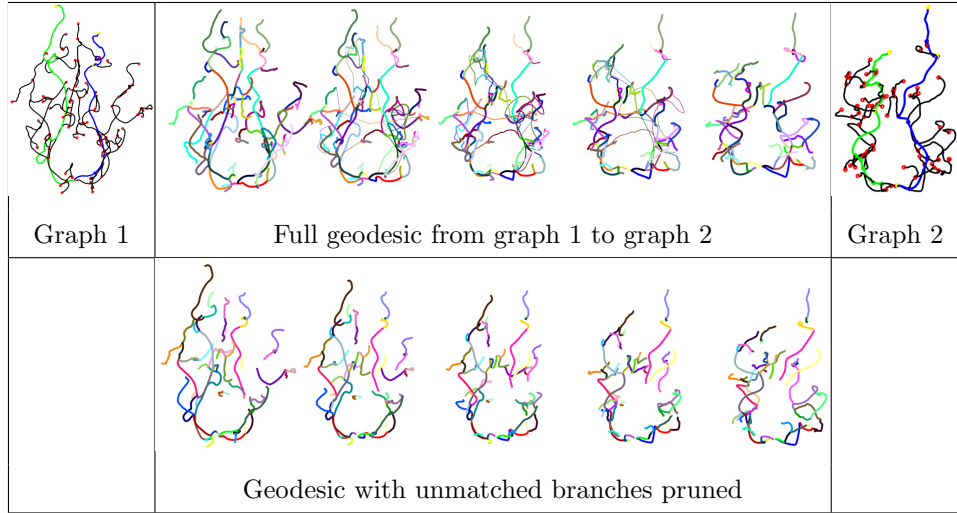


Figure 15: Geodesic path between two BANs (bottom components) using five registered landmarks.

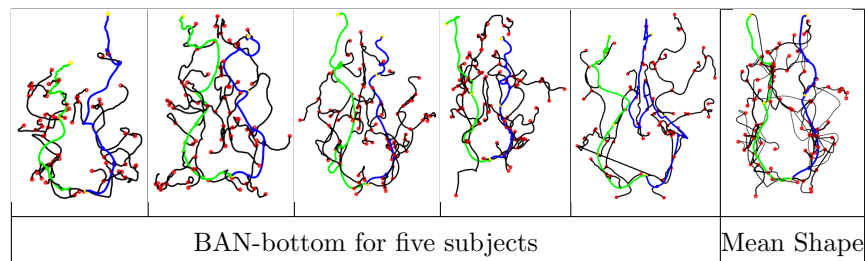


Figure 16: Sample mean of BAN components using improved landmark-based registration.

6 Conclusion

This paper develops techniques for representing and statistically analyzing shapes of Brain Arterial Networks or BANs, broken into four major components. These objects – BANs components – are complex due to arbitrary numbers, shapes, sizes, and connectivities of 3D arterial curves forming these networks. We represent them using elastic graphs and their adjacency matrices, where entries in adjacency matrices are the shapes of the corresponding edges (arteries). We solve for registration of nodes across graphs between compared and use the geometry of the shape space to compute geodesics, sample means, PCA components of BANs. The sample means help capture prominent common characteristics of different BANs while covariance-PCA analysis helps represent individual variability in a tractable fashion.

The subsequent data analysis shows that age has a significant effect on three components of BANs – left, right, and bottom – but has no effect on the top component. We use the tools developed here to visualize the nature of BAN shape variability resulting from aging. In fact visualization of shapes along principal directions or age-regression directions are important accomplishments of this framework. One can pinpoint arteries that undergo significant deformations and arteries that don't change much over time.

The overall performance of this framework relies on the quality of registration of nodes across graphs. For very large graphs, the current computational tools may not be sufficient and one needs to explore new ideas. Landmark-guided registration is proposed as a solution to that problem.

Acknowledgements

This research was supported in part by the grants NIH R01 MH120299, NSF DMS 1621787, and NSF DMS 1953087.

References

- [1] Burcu Aydin, Gábor Pataki, Haonan Wang, Elizabeth Bullitt, James Stephen Marron, et al. A principal component analysis for trees. *The Annals of Applied Statistics*, 3(4):1597–1615, 2009.
- [2] Stephen R Aylward and Elizabeth Bullitt. Initialization, noise, singularities, and scale in height ridge traversal for tubular object centerline extraction. *IEEE transactions on medical imaging*, 21(2):61–75, 2002.
- [3] Paul Bendich, James S Marron, Ezra Miller, Alex Pieloch, and Sean Skwerer. Persistent homology analysis of brain artery trees. *The annals of applied statistics*, 10(1):198, 2016.
- [4] Elizabeth Bullitt, Donglin Zeng, Guido Gerig, Stephen Aylward, Sarang Joshi, J Keith Smith, Weili Lin, and Matthew G Ewend. Vessel tortuosity and brain tumor malignancy: a blinded study1. *Academic radiology*, 12(10):1232–1240, 2005.
- [5] Elizabeth Bullitt, Donglin Zeng, Benedicte Mortamet, Arpita Ghosh, Stephen R Aylward, Weili Lin, Bonita L Marks, and Keith Smith. The effects of healthy aging on intracerebral blood vessels visualized by magnetic resonance angiography. *Neurobiology of aging*, 31(2):290–300, 2010.
- [6] Terry Caelli and Serhiy Kosinov. An eigenspace projection clustering method for inexact graph matching. *IEEE transactions on pattern analysis and machine intelligence*, 26(4):515–519, 2004.
- [7] Anna Calissano, Aasa Feragen, and Simone Vantini. Populations of unlabeled networks: Graph space geometry and geodesic principal components. 2020.
- [8] Samir Chowdhury and Tom Needham. Gromov-wasserstein averaging in a riemannian framework. In *The IEEE/CVF Conference on Computer Vision and Pattern Recognition (CVPR) Workshops*, June 2020.
- [9] Timothee Cour, Praveen Srinivasan, and Jianbo Shi. Balanced graph matching. In *Advances in Neural Information Processing Systems*, pages 313–320, 2007.

[10] Ian L Dryden and Kanti V Mardia. *Statistical shape analysis: with applications in R*, volume 995. John Wiley & Sons, 2016.

[11] Adam Duncan, Eric Klassen, Anuj Srivastava, et al. Statistical shape analysis of simplified neuronal trees. *The Annals of Applied Statistics*, 12(3):1385–1421, 2018.

[12] Donniell E Fishkind, Sancar Adali, Heather G Patsolic, Lingyao Meng, Digvijay Singh, Vince Lyzinski, and Carey E Priebe. Seeded graph matching. *arXiv preprint arXiv:1209.0367*, 2012.

[13] Steven Gold and Anand Rangarajan. A graduated assignment algorithm for graph matching. *IEEE Transactions on pattern analysis and machine intelligence*, 18(4):377–388, 1996.

[14] Xiaoyang Guo, Anuj Srivastava, and Sudeep Sarkar. A quotient space formulation for statistical analysis of graphical data. *arXiv preprint arXiv:1909.12907*, 2019.

[15] Charles Hagwood, Javier Bernal, Michael Halter, John Elliott, and Tegan Brennan. Testing equality of cell populations based on shape and geodesic distances. *IEEE Transactions on Medical Imaging*, 32(12), 2013.

[16] AD Hoover, Valentina Kouznetsova, and Michael Goldbaum. Locating blood vessels in retinal images by piecewise threshold probing of a matched filter response. *IEEE Transactions on Medical imaging*, 19(3):203–210, 2000.

[17] Brijnesh J Jain and Klaus Obermayer. Structure spaces. *Journal of Machine Learning Research*, 10(Nov):2667–2714, 2009.

[18] Brijnesh J Jain and Klaus Obermayer. Graph quantization. *Computer Vision and Image Understanding*, 115(7):946–961, 2011.

[19] Brijnesh J Jain and Klaus Obermayer. Learning in riemannian orbifolds. *arXiv preprint arXiv:1204.4294*, 2012.

[20] Ian H Jermyn, Sebastian Kurtek, Eric Klassen, and Anuj Srivastava. Elastic shape matching of parameterized surfaces using square root normal fields. In *European conference on computer vision*, pages 804–817. Springer, 2012.

[21] Ian H Jermyn, Sebastian Kurtek, Hamid Laga, and Anuj Srivastava. Elastic shape analysis of three-dimensional objects. *Synthesis Lectures on Computer Vision*, 12(1):1–185, 2017.

[22] D. G. Kendall, D. Barden, T. K. Carne, and H. Le. *Shape and shape theory*. Wiley, 1999.

[23] David G Kendall. Shape manifolds, procrustean metrics, and complex projective spaces. *Bulletin of the London mathematical society*, 16(2):81–121, 1984.

[24] Eric Klassen, Anuj Srivastava, M Mio, and Shantanu H Joshi. Analysis of planar shapes using geodesic paths on shape spaces. *IEEE transactions on pattern analysis and machine intelligence*, 26(3):372–383, 2004.

[25] Jee-Hyun Kong, Daniel R Fish, Rebecca L Rockhill, and Richard H Masland. Diversity of ganglion cells in the mouse retina: unsupervised morphological classification and its limits. *Journal of Comparative Neurology*, 489(3):293–310, 2005.

[26] Tjalling C Koopmans and Martin Beckmann. Assignment problems and the location of economic activities. *Econometrica: journal of the Econometric Society*, pages 53–76, 1957.

[27] Eugene L Lawler. The quadratic assignment problem. *Management science*, 9(4):586–599, 1963.

[28] Alice LeBrigand. A discrete framework to find the optimal matching between manifold-valued curves. *61(1):40–70*, 2019.

[29] Marius Leordeanu and Martial Hebert. A spectral technique for correspondence problems using pairwise constraints. In *Tenth IEEE International Conference on Computer Vision (ICCV'05) Volume 1*, volume 2, pages 1482–1489. IEEE, 2005.

[30] Marius Leordeanu, Martial Hebert, and Rahul Sukthankar. An integer projected fixed point method for graph matching and map inference. In *Advances in neural information processing systems*, pages 1114–1122, 2009.

[31] Zhi-Yong Liu, Hong Qiao, and Lei Xu. An extended path following algorithm for graph-matching problem. *IEEE transactions on pattern analysis and machine intelligence*, 34(7):1451–1456, 2012.

[32] Dan Shen, Haipeng Shen, Shankar Bhamidi, Yolanda Muñoz Maldonado, Yongdai Kim, and J Stephen Marron. Functional data analysis of tree data objects. *Journal of Computational and Graphical Statistics*, 23(2):418–438, 2014.

[33] C. G. Small. *The Statistical Theory of Shape*. Springer, 1996.

[34] Anne Sonnenschein, David VanderZee, William R Pitchers, Sudarshan Chari, and Ian Dworkin. An image database of drosophila melanogaster wings for phenomic and biometric analysis. *GigaScience*, 4(1):25, 2015.

[35] Anuj Srivastava, Eric Klassen, Shantanu H Joshi, and Ian H Jermyn. Shape analysis of elastic curves in euclidean spaces. *IEEE Transactions on Pattern Analysis and Machine Intelligence*, 33(7):1415–1428, 2011.

[36] Anuj Srivastava and Eric P Klassen. *Functional and shape data analysis*. Springer, 2016.

[37] Shinji Umeyama. An eigendecomposition approach to weighted graph matching problems. *IEEE transactions on pattern analysis and machine intelligence*, 10(5):695–703, 1988.

[38] Joshua T Vogelstein, John M Conroy, Vince Lyzinski, Louis J Podrazik, Steven G Kratzer, Eric T Harley, Donniell E Fishkind, R Jacob Vogelstein, and Carey E Priebe. Fast approximate quadratic programming for graph matching. *PLOS one*, 10(4):e0121002, 2015.

[39] Guan Wang, Hamid Laga, Jinyuan Jia, Stanley J Miklavcic, and Anuj Srivastava. Statistical analysis and modeling of the geometry and topology of plant roots. *Journal of Theoretical Biology*, 486:110108, 2020.

[40] Larry Wasserman. Topological data analysis. *Annual Review of Statistics and Its Application*, 5:501–532, 2018.

[41] Junchi Yan, Xu-Cheng Yin, Weiyao Lin, Cheng Deng, Hongyuan Zha, and Xiaokang Yang. A short survey of recent advances in graph matching. In *Proceedings of the 2016 ACM on International Conference on Multimedia Retrieval*, pages 167–174, 2016.

[42] L. Younes. Computable elastic distance between shapes. *SIAM Journal of Applied Mathematics*, 58:565–586, 1998.

[43] L. Younes, P. W. Michor, J. Shah, D. Mumford, and R. Lincei. A metric on shape space with explicit geodesics. *Matematica E Applicazioni*, 19(1):25–57, 2008.

[44] Andrei Zanfir and Cristian Sminchisescu. Deep learning of graph matching. In *Proceedings of the IEEE Conference on Computer Vision and Pattern Recognition*, pages 2684–2693, 2018.

[45] Zhengwu Zhang, Eric Klassen, and Anuj Srivastava. Phase-amplitude separation and modeling of spherical trajectories. *Journal of Computational and Graphical Statistics*, 27(1):85–97, 2018.

[46] Feng Zhou and Fernando De la Torre. Factorized graph matching. In *2012 IEEE Conference on Computer Vision and Pattern Recognition*, pages 127–134. IEEE, 2012.

[47] Feng Zhou and Fernando De la Torre. Factorized graph matching. *IEEE transactions on pattern analysis and machine intelligence*, 38(9):1774–1789, 2015.